Microelectronic Engineering 88 (2011) 377–382

Contents lists available at ScienceDirect

Microelectronic Engineering

journal homepage: www.elsevier.com/locate/mee

Scanning tunneling microscopy study of the interfacial bonding structures of Ga_2O and $In_2O/In_{0.53}Ga_{0.47}As(0\,0\,1)$

Jian Shen [a,b,*], Darby L. Feldwinn [b], Wilhelm Melitz [a,b], Ravi Droopad [c], Andrew C. Kummel [b]

[a] *Materials Science & Engineering Program, University of California, San Diego, La Jolla, CA 92093, USA*
[b] *Department of Chemistry and Biochemistry, University of California, San Diego, La Jolla, CA 92093, USA*
[c] *Department of Physics, Texas State University, San Marcos, TX 78666, USA*

ARTICLE INFO

Article history:
Available online 25 October 2010

Keywords:
Surface reconstruction
III–V Compound semiconductor
MOSFET
Semiconductor-oxide interface
Scanning tunneling microscopy

ABSTRACT

Ga_2O and In_2O oxides were deposited on $In_{0.53}Ga_{0.47}As(0\,0\,1)-(4\times2)$ surface by a high temperature effusion cell to investigate the interfacial bonding geometries and electronic structures by scanning tunneling microscopy/spectroscopy (STM/STS). At low coverage, Ga_2O molecules bond to the As atoms at the edge of the rows and preexisting Ga_2O on the surface. Annealing the $Ga_2O/In_{0.53}Ga_{0.47}As(0\,0\,1)-(4\times2)$ to 340 °C results in formation of slightly ordered islands running in the [1 1 0] direction and rectangle shape flat islands on the surface. At high coverage with 340 °C post-deposition annealing (PDA), Ga_2O oxides form disordered structures with the large flat terraces on the surface. Conversely, at high coverage with 380 °C PDA, In_2O on $In_{0.53}Ga_{0.47}As(0\,0\,1)-(4\times2)$ forms ordered structures running in the [1 1 0] direction. STS results show that Ga_2O oxide does not passivate the interface nor unpin the $In_{0.53}Ga_{0.47}As(0\,0\,1)-(4\times2)$ surface consistent with its inability to form monolayer ordered islands on the surface; conversely, $In_2O/In_{0.53}Ga_{0.47}As(0\,0\,1)-(4\times2)$ has an ordered monolayer coverage and is unpinned.

1. Introduction

The semiconductor industry has been geometrically scaling the physical dimensions of complementary metal oxide semiconductor (CMOS) devices. Silicon based metal-oxide semiconductor field-effect transistor (MOSFET) technology is rapidly approaching its physical limits. Alternative materials may be required to continue the progress in device scaling predicted by Moore's Law. InGaAs and related III–V compound semiconductors might provide a solution because they exhibit ~5–20 times higher effective channel mobility than silicon [1,2]. The key to fabricating a practical III–V MOSFET is forming an unpinned oxide/semiconductor interface with low fixed charge and low trap density [3]. Fermi level pinning can be caused by strong perturbations to the electronic structure of the oxide/semiconductor interface inducing formation of interface trap states which degrade device performance [4,5]. These perturbations can be caused by formation of localized charges [6], interface dipoles [7], or dangling bonds [8]. In order to obtain a fundamental understanding of surface passivation of III–V compound semiconductors, it is critical to investigate and understand the oxide/semiconductor interface bonding at the atomic level.

In this study, oxide morphologies and the possible bonding geometries of two different oxides, Ga_2O and In_2O, on group III rich $In_{0.53}Ga_{0.47}As\ (0\,0\,1)-(4\times2)$ along with the electronic structure of Ga_2O on $In_{0.53}Ga_{0.47}As(0\,0\,1)$ were explored. Scanning tunneling microscopy (STM) was used to determine the interfacial bonding structure of Ga_2O and In_2O on $In_{0.53}Ga_{0.47}As(0\,0\,1)-(4\times2)$ after the room temperature oxide deposition and post-deposition annealing (PDA). Density functional theory (DFT) simulation is used to model the bonding structures that are observed by STM so that the cause of the Fermi level pinning and unpinning can be determined. Scanning tunneling spectroscopy (STS) measurements were performed to determine the Fermi level of the $Ga_2O/In_{0.53}Ga_{0.47}As(0\,0\,1)-(4\times2)$ interface; the STS of the Fermi level of the $In_2O/In_{0.53}Ga_{0.47}As(0\,0\,1)-(4\times2)$ interface was also measured but previously reported [9].

2. Experimental method

Molecular beam epitaxy (MBE) was employed to grow 200 nm of $1\times10^{18}\,cm^{-3}$ doped $In_{0.53}Ga_{0.47}As$ on 2 inch $InP(0\,0\,1)$ $1\times10^{18}\,cm^{-3}$ doped substrates (both *p*-type and *n*-type). A mixture of As2 and As4 was used as the group V species. Si and Be were used as *n*- and *p*-type dopants. The growth rate of $In_{0.53}Ga_{0.47}As$ was 0.4 ML/s, determined by reflection high-energy electron diffraction (RHEED) intensity oscillations, at a temperature just below

---

[*] Corresponding author. Present address: Intel Corporation, Chandler, AZ 85226, USA.

E-mail address: jian.az.shen@intel.com (J. Shen).

doi:10.1016/j.mee.2010.10.023

the transition of the (2 × 4) to the (4 × 2) surface. The wafers were capped, in situ, with a 50 nm protective As_2 cap. The wafers were transferred to a vacuum container for transporting to the STM chamber. The STM chamber is equipped with low energy electron diffraction (LEED), a high temperature effusion cell, and an Omicron variable temperature STM. The As capped wafers were radiatively heated to obtain the $In_{0.53}Ga_{0.47}As(0\,0\,1) - (2 \times 4)$ or (4 × 2) reconstruction. After the (2 × 4) or (4 × 2) surface reconstruction was verified by LEED, the sample was transferred to the STM. STM images were taken at room temperature using constant-current mode. Subsequently, Ga_2O was deposited by evaporating sintered $Ga_2O3(s)$ from high temperature effusion cell contained in a differentially pumped chamber.

Fig. 1 shows a schematic diagram of the oxide deposition setup used in this experiment. $Ga_2O3(s)$ sublimates as $Ga_2O(g)$ and $O_2(g)$ at 1485 °C [3]. However due to the low sticking probability of O_2 on group III-rich (4 × 2) surfaces, the majority of the adsorbing species are Ga_2O. An identical deposition system was used for In_2O.

The major technique used for characterizing the morphological and electronic structure of surfaces and interfaces with atomic resolution is scanning tunneling microscopy (STM) [10–14]. STM can be used to image both the clean semiconductor surfaces and adsorbate covered semiconductor surfaces thereby facilitating initial assignments of adsorbate/semiconductor bonding sites. The basic mechanism of STM imaging is illustrated in Fig. 2; only three components are considered: tip, vacuum space, and sample. When the tip is brought very close to the sample (~10 Å) and a voltage is applied between the tip and sample, the electrons will tunnel through the vacuum barrier. This tunneling current is given approximately by

$$I \propto V e^{-kz} \tag{1}$$

where V is the applied voltage between the tip and the sample, k is the decay length and z is the tunneling gap between the tip and the sample surface. The exponential decay dependence between the tunneling current and the tunneling gap is the source of the high depth resolution of STM. In constant current mode imaging, the tip scans across the sample surface in the x and y directions as the current is measured while a feedback loop moves tip in the vertical direction (z) to maintain the constant tunneling current value. By recording the vertical movement of the scanning tip, the sample topography can be imaged and the atomic level surface structure can be studied. Normally, the measured equal-current contour lines are interpreted as real space surface topography. However, the STM image is actually a convolution of the electronic and topographic structure of sample surface since STM probes surface charge density [15]. The other STM imaging mode is constant height where the tip height is held constant and current changes are imaged. In the studies described in this paper, only constant current mode was used.

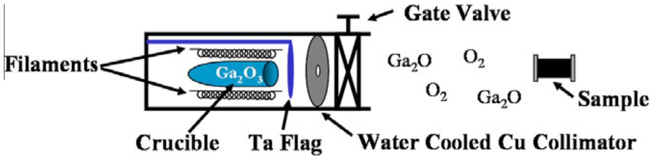

Fig. 1. A schematic diagram of the oxide deposition system. Ga_2O was deposited by evaporating sintered $Ga_2O_3(s)$ from a high temperature effusion cell contained in a differentially pumped chamber. $Ga_2O_3(s)$ sublimates as $Ga_2O(g)$ and $O_2(g)$ at 1485° [3]. However due to the low sticking probability of O_2 on group III-rich (4 × 2) surfaces, the majority of the adsorbing species are Ga_2O.

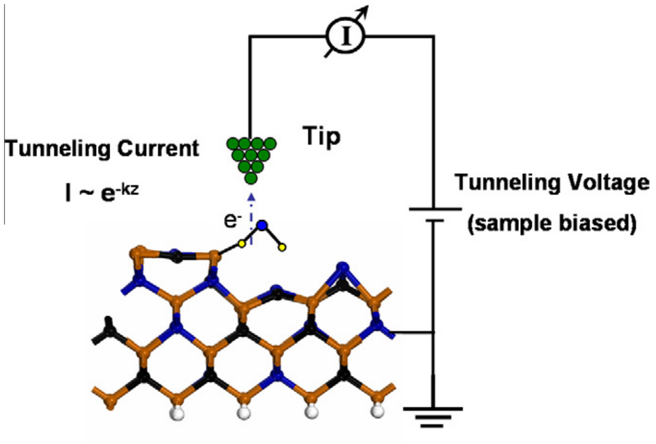

Fig. 2. Schematic diagram of an STM of the oxide deposited III–V semiconductor surface.

The STM image is not just a topographical image of sample surface because the tunneling current strongly depends on the electronic density of states (DOS) of the surface. Scanning tunneling spectroscopy (STS) is employed to directly measure the DOS using the STM apparatus. When a negative bias is applied to the tip relative to the sample, the electrons will tunnel from tip states through vacuum barrier into empty states of the sample surface. When a positive bias is applied to the tip relative to the sample, the electrons will tunnel from filled states of sample surface through vacuum barrier into the tip. Therefore, information concerning the sample's surface states can be obtained by ramping the applied voltage from negative to positive biases. According to Tersoff's tunneling theory [16,17], the differential conductance (dI/dV) spectra measurement can provide very useful information concerning the electronic structure of sample surface, including the local density of states (LDOS) of the surface at a particular energy. Detailed descriptions of the STS technique have been published by Feenstra et al. and Tersoff et al. [16–21]. Filled state constant current STM images were generally taken at −3 to −1.5 V sample bias and 0.1–0.25 nA tunneling current with electrochemically etched tungsten tips. For STS, generally a 50 mV amplitude and 1.5 kHz sinusoidal modulation voltage is superimposed on the tip bias, and the dI/dV spectra is recorded using a DSP lock-in amplifier (Signal Recovery 7280).

3. Results and discussion

3.1. Surface reconstruction

$In_{0.53}Ga_{0.47}As(0\,0\,1)$ surface has several different reconstructions [22–24]. For our decapping and annealing method, there are three temperature regions for different surface reconstructions as shown in Table 1. Fig. 3 shows 300 K STM images of clean $In_{0.53}Ga_{0.47}As(0\,0\,1)$ surfaces with these three different reconstructions from three different annealing (PDA) temperatures: (a) for 330–400 °C annealing temperature, the surface has mainly the α2(2 × 4) reconstruction with small regions of β2(2 × 4) reconstructions; (b) for 400–440 °C annealing temperature, the surface has a mixture of (2 × 4)/(4 × 2) reconstructions; (c) for >450 °C annealing temperature, nearly all regions have the (4 × 2) reconstruction. The (2 × 4) surface reconstructions have a top row of dimerized As atoms running in the $[\bar{1}\,1\,0]$ direction which are

Table 1
Annealing temperature regions for different surface reconstructions.

Reconstruction	As rich (2 × 4)	Mixed (2 × 4) and (4 × 2)	In/Ga rich (4 × 2)
Annealing temperature (°C)	330–400	400–440	>450

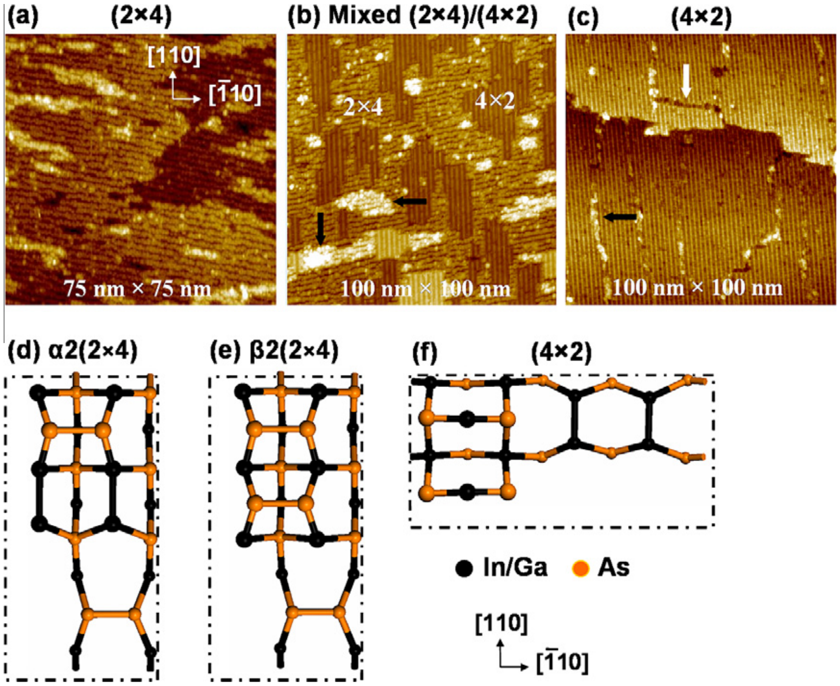

Fig. 3. Filled state STM images taken at 300 K of the $In_{0.53}Ga_{0.47}As(0\,0\,1)$ surface with schematic diagrams for three different reconstructions (Filled state STM image with $Vs = -2$ V, $It = 0.1$ nA). (a) 380 °C annealed As rich InGaAs(0 0 1) – (2 × 4). (b) 430 °C annealed mixed (2 × 4) and (4 × 2); (2 × 4) and (4 × 2) surface regions are marked. The 2 × 4 regions have nearly horizontal rows running in the [$\bar{1}$ 1 0] direction while the 4 × 2 regions have nearly vertical rows running in the [1 1 0] direction; the black arrows show the second layer (2 × 4) surface structure. (c) 460 °C annealed In/Ga rich InGaAs(0 0 1) – (4 × 2). (d) InGaAs(0 0 1)-α2(2 × 4) has As row and trough dimers and In/Ga edge dimers. (e) InGaAs(0 0 1)-β2(2 × 4) has row and trough As dimers. (f) InGaAs(0 0 1) – (4 × 2) has undimerized row and In/Ga trough dimers. Note that for (2 × 4) structure, STM image shows most of areas are α2(2 × 4), and a few of them are β2(2 × 4).

bonded to tricoordinated In/Ga atoms. Between the As rows are trough regions that contains one As dimer per unit cell. The main difference between the α2(2 × 4) and β2(2 × 4) structures is that α2 structure has single As dimer on the row [Fig. 3(d)] and the β2 structure has double As dimers on the row [Fig. 3(e)]. In addition, the α2 reconstruction has two degenerate reconstructions; the As dimer can either be on the left or the right of the row. This degeneracy causes the surface structure appears to have rows that are not completely straight in STM images shown in Fig. 3(a). The (4 × 2) surface reconstruction has a top row of In/Ga atoms running in the [1 1 0] direction. Between the In/Ga rows are trough regions that contains two In/Ga dimer per unit cell. The mixed (2 × 4) and (4 × 2) STM image shown in Fig. 3(b) has (4 × 2) row feature running in the [1 1 0] direction and (2 × 4) row feature running in the [$\bar{1}$ 1 0] direction. The bright features shown in Fig. 3(b) as the black arrows are the second layer (2 × 4) surface reconstruction, which are not the surface defects. For the (4 × 2) surface shown in Fig. 3(c), there are at least four kinds of defects on the surface: dark cuts on the row, protrusion dots between the rows which are shown in the high resolution image, domain boundaries as depression lines in the [$\bar{1}$ 1 0] direction denoted by the white arrow, and domain boundaries as protrusion lines in the [1 1 0] direction denoted by the black arrow.

Since the As-rich reconstruction contains a mixture of surface reconstructions, the current study focuses on the In/Ga-rich (4 × 2) reconstruction. Even if a pure As-rich (2 × 4) reconstruction could be generated, there are additional advantages to performing experiments on the In/Ga rich (4 × 2) reconstruction. The (2 × 4) surface contains As dimers which are readily displaced by O_2 [25] or form arsenic oxides. These excess arsenic or arsenic oxides on the surface can be responsible for surface Fermi level pinning [5,26]. The In/Ga rich reconstruction was chosen for oxide/InGaAs bonding structure study because it is resistant to oxidation due to the absence of As dimers on In/Ga-rich (4 × 2) surface.

3.2. $Ga_2O/In_{0.53}Ga_{0.47}As$ bonding

Ga_2O was deposited on the surface to determine the oxide bonding structure on the $In_{0.53}Ga_{0.47}As(0\,0\,1) – (4 \times 2)$ surface. When $Ga_2O3(s)$ is evaporated from a high temperature effusion cell, it forms $Ga_2O(g)$ and $O_2(g)$ at 1485 °C [3]. The $O_2(g)$ does not stick on the room temperature $In_{0.53}Ga_{0.47}As(0\,0\,1) – (4 \times 2)$ clean surface so $In_{0.53}Ga_{0.47}As$ is covered with $Ga_2O(s)$. The deposition rate was estimated as 0.04 ML/min based on the known deposition time and using STM to measure the oxide coverage and oxide height after PDA (1–1.2 Å/layer). Deposition at room temperature results in a nearly amorphous structure. At low coverage, the most probable chemisorption sites are Ga_2O molecules bonding to the As atoms at the edge of the rows with an oxide height of about 1.6 Å between the oxide and the rows of the clean surface shown in Fig. 4e; in addition, the Ga_2O molecules bonding with preexisting Ga_2O on the surface have an oxide height of about 2.5 Å between the oxide and the rows of the clean surface shown in Fig. 4f. At medium coverage, a 340 °C PDA results in formation of slightly ordered islands running in the [$\bar{1}$ 1 0] direction; rectangle shape flat islands are observed with an oxide height of 1–1.2 Å. At high coverage with 340 °C PDA, Ga_2O oxides form disordered structures with large flat terraces on the surface. While the height of the high coverage oxide islands with 340 °C PDA cannot be directly determined since the surface is completely covered with oxide, the step edge height of Ga_2O deposited $In_{0.53}Ga_{0.47}As(0\,0\,1) – (4 \times 2)$ is the same as on clean $In_{0.53}Ga_{0.47}As(0\,0\,1) – (4 \times 2)$ surface (~2.8 Å) consistent with the theoretical step edge value for $In_{0.53}Ga_{0.47}As(0\,0\,1)$ surface (half lattice constant, 2.93 Å). RMS roughness for the high coverage of Ga_2O deposited $In_{0.53}Ga_{0.47}As(0\,0\,1) – (4 \times 2)$ is about 1.2 Å. The ~2.8 Å step edge height and the low RMS roughness are consistent with the 340 °C PDA high coverage islands having the same structure and height (1–1.2 Å) as the 340 °C PDA medium coverage islands. The bonding structure of the annealed Ga_2O deposited on

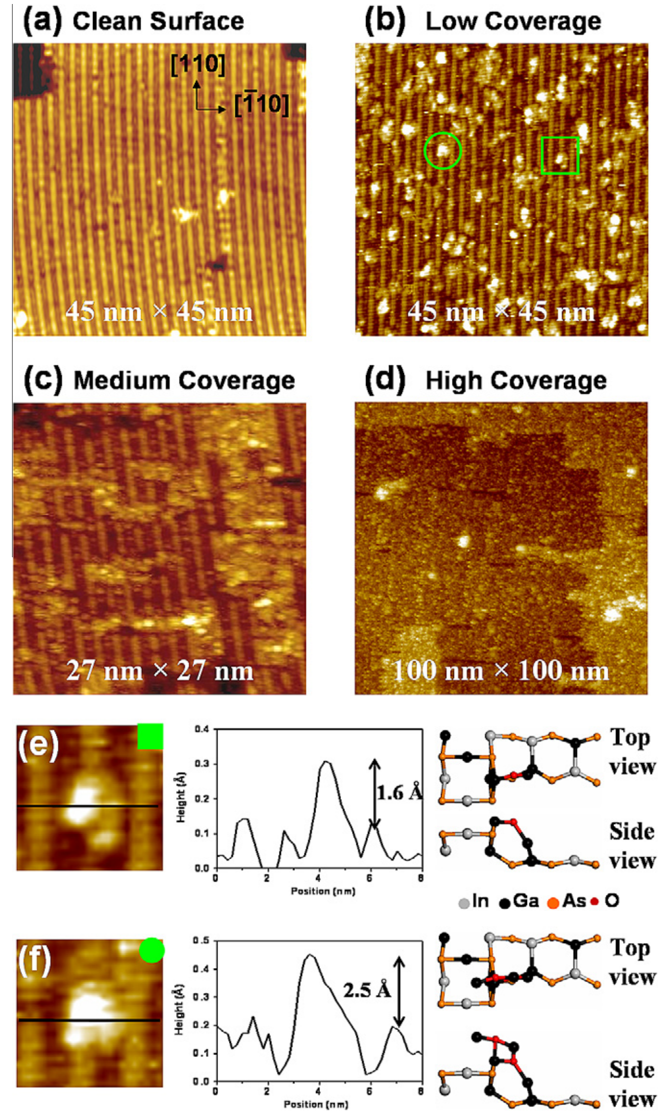

Fig. 4. Filled state STM images of Ga_2O deposited $In_{0.53}Ga_{0.47}As(0\,0\,1) - (4 \times 2)$ surface at 300 K. (a) Clean $In_{0.53}Ga_{0.47}As(0\,0\,1) - (4 \times 2)$ surface. (b) Low coverage of Ga_2O on $In_{0.53}Ga_{0.47}As(0\,0\,1) - (4 \times 2)$ with 110 °C PDA; the square outlines the most probable chemisorption site with an oxide height about 1.6 Å between the oxide and the rows of the clean surface, and the circle outlines a common site with an oxide height about 2.5 Å between the oxide and the rows of the clean surface. (c) Medium coverage of Ga_2O on $In_{0.53}Ga_{0.47}As(0\,0\,1) - (4 \times 2)$ with 340 °C PDA. (d) High coverage of Ga_2O on $In_{0.53}Ga_{0.47}As(0\,0\,1) - (4 \times 2)$ with 340 °C PDA. Two expanded STM images from the low coverage dose with 110 °C PDA illustrate two different heights with corresponding geometric symbols, line scan corresponding to the black line on the STM image, and possible bonding structures: (e) a Ga_2O molecule bonds to the As atoms at the edge of the rows and forms new Ga–As bonds; 1.6 Å oxide height, and (f) a Ga_2O molecule bonds with a preexisting Ga_2O on the surface and forms new Ga–O bonds; 2.5 Å oxide height.

$In_{0.53}Ga_{0.47}As(0\,0\,1) - (4 \times 2)$ looks different than the bonding structure of In_2O deposited on $In_{0.53}Ga_{0.47}As(0\,0\,1) - (4 \times 2)$.

3.3. $In_2O/In_{0.53}Ga_{0.47}As$ bonding

When $In_2O3(s)$ is evaporated from a high temperature effusion cell, it forms $In_2O(g)$ and $O_2(g)$ at 1000–1025 °C [27]. The deposition rate was estimated as 0.06 ML/min based on the known deposition time and using STM to measure the oxide coverage and oxide height after PDA (1–1.2 Å/layer). Similar to Ga_2O deposition, the $O_2(g)$ does not readily stick on the room temperature $In_{0.53}Ga_{0.47}As(0\,0\,1) - (4 \times 2)$ clean surface so $In_{0.53}Ga_{0.47}As$ is covered with $In_2O(s)$. A filled-state STM image shown in Fig. 5a reveals that at low coverage, In_2O molecules mainly occupy single sites at the edge of the rows [9]. The In_2O most likely form new In–As bonds to the surface as shown by detailed STM imaging and DFT modeling studies [9]. Fig. 5d shows the expanded STM image from Fig. 5a with corresponding hexagon symbol, line scan corresponding to the black line on the STM image, and possible bonding structure. At medium coverage with 380 °C PDA, an ordered oxide surface structure was observed. Comparisons of oxide height difference before and after annealing show that the height difference between deposited In_2O oxide and surface rows is reduced from 1.5 to 1–1.2 Å. It is likely that the annealed In_2O molecules no longer bond just with the row edge As atoms but also form new O–In/Ga bonds in the trough thereby reducing the oxide height difference as confirmed by density function theory (DFT) calculations [9]. For the full coverage with 380 °C PDA, the In_2O oxide forms ordered structures running in the [1 1 0] direction on $In_{0.53}Ga_{0.47}As(0\,0\,1) - (4 \times 2)$ surface, which is completely different than that of Ga_2O deposited on $In_{0.53}Ga_{0.47}As(0\,0\,1) - (4 \times 2)$. It is noted that there is substantial amount of second layer growth with 0.9 Å RMS roughnesses probably due to In_2O–In_2O interactions, but these are sufficiently weak to allow full coverage formation of an In_2O overlayer.

A possible reason for the lack of order for $Ga_2O/In_{0.53}Ga_{0.47}As(0\,0\,1) - (4 \times 2)$ is the Ga_2O molecules forming strong bonds to $In_{0.53}Ga_{0.47}As(0\,0\,1) - (4 \times 2)$ as well as strong oxide–oxide bonds thereby inhibiting diffusion. DFT calculations have been performed for Ga_2O and In_2O on As-rich $InGaAs(0\,0\,1) - (2 \times 4)$ showing that the bonding energies are −1.86 eV/Ga_2O and −1.12 eV/In_2O for the row insertion sites [28]; while the bonding sites are different on In/Ga-rich $InGaAs(0\,0\,1) - (4 \times 2)$ a similar difference in bonding energies is expected for Ga_2O and In_2O on $InGaAs(0\,0\,1) - (4 \times 2)$ since Ga–As bonds are stronger than In–As bonds consistent with the lower diffusion of Ga_2O than that of In_2O on $InGaAs(0\,0\,1) - (4 \times 2)$.

3.4. Electronic structure

Scanning tunneling spectroscopy (STS) was used to measure the electronic structure of the surface. The STS of the clean surface shows the Fermi level pinning (see blue curves shown in Fig. 6). Both the clean *n*-type and *p*-type samples have a Fermi level (0 V position in STS) at the valence band edge. The Fermi level shift for *n*-type sample may be caused by surface states [24]. After Ga_2O deposition and annealing, the STS spectra does not change as shown in by green curves; this is consistent with Ga_2O not electronically passivating the interface and $Ga_2O/In_{0.53}Ga_{0.47}As(0\,0\,1) - (4 \times 2)$ surface being pinned. For $In_2O/In_{0.53}Ga_{0.47}As(0\,0\,1) - (4 \times 2)$, the Fermi level position is close to the conduction band minimum (CBM) for *n*-type samples while close to the valence band maximum (VBM) for *p*-type samples, which is consistent with an unpinned surface. The detailed STS results of $In_2O/In_{0.53}Ga_{0.47}As$ are discussed elsewhere [9]. It is possible that the low diffusivity of Ga_2O on the high defect density $In_{0.53}Ga_{0.47}As(0\,0\,1) - (4 \times 2)$ surface prevents formation of oxide islands with sufficient order and coverage to remove the surface dipole and create an unpinned surface. Ga_2O deposited on $GaAs(0\,0\,1) - (2 \times 4)$ is a good example for unpinning. Hale et al. have reported STM/STS results of Ga_2O deposited on $GaAs(0\,0\,1) - (2 \times 4)$ [3]. STS results show for Ga_2O deposited on *n*-type $GaAs(0\,0\,1) - (2 \times 4)$ samples, the Fermi level position is close to CBM consistent with unpinning in contrast with Ga_2O deposited on *n*-type $InGaAs(0\,0\,1) - (4 \times 2)$. STM results show Ga_2O oxide forms monolayer ordered structure on $GaAs(0\,0\,1) - (2 \times 4)$ in which the Ga_2O inserts into As–As bonds to restore the surface to bulk-like termination. Since there are no As–As dimers on the $InGaAs(0\,0\,1) - (4 \times 2)$ surface, the Ga_2O As

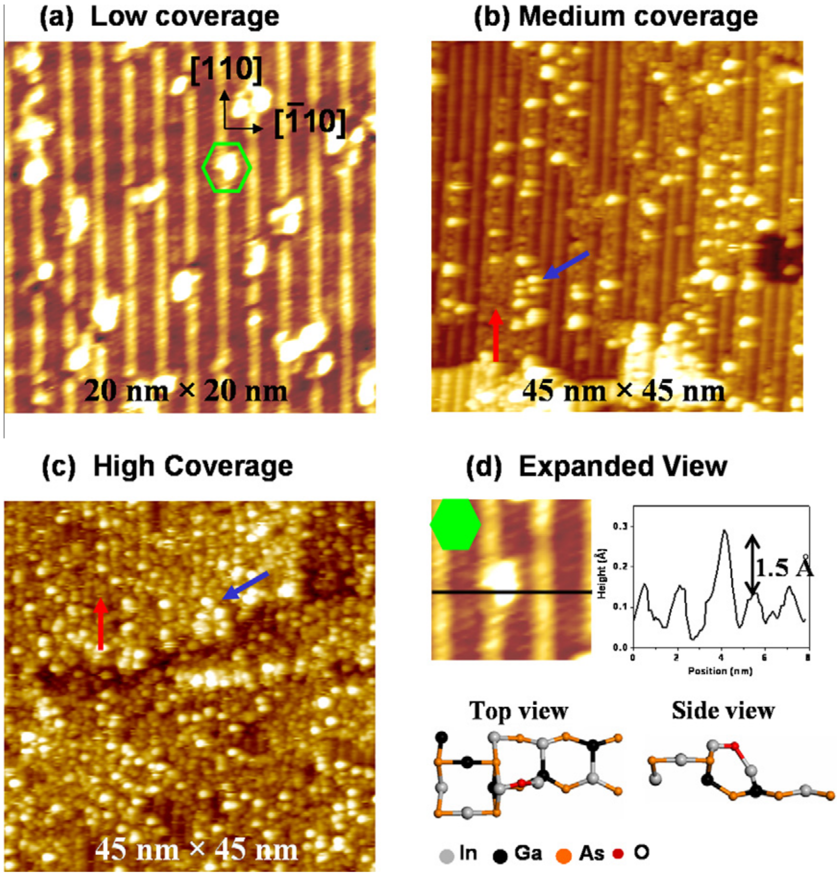

Fig. 5. In_2O deposited $In_{0.53}Ga_{0.47}As(0\,0\,1) - (4 \times 2)$ surface. (a) Low coverage of In_2O on $In_{0.53}Ga_{0.47}As(0\,0\,1) - (4 \times 2)$. (b) Medium coverage of In_2O on $In_{0.53}Ga_{0.47}As(0\,0\,1) - (4 \times 2)$ with 380 °C PDA. The first layer sites are yellow (red arrow), while the second layer sites are white (blue arrow). (c) High coverage of In_2O on $In_{0.53}Ga_{0.47}As(0\,0\,1) - (4 \times 2)$ with 380 °C PDA. The first layer sites are yellow (red arrow), while the second layer sites are white (blue arrow). (d) Expanded STM image from Fig. 5a with corresponding hexagon symbol, line scan corresponding to the black line on the STM image, and possible bonding structure. (For interpretation of the references to colour in this figure legend, the reader is referred to the web version of this article.)

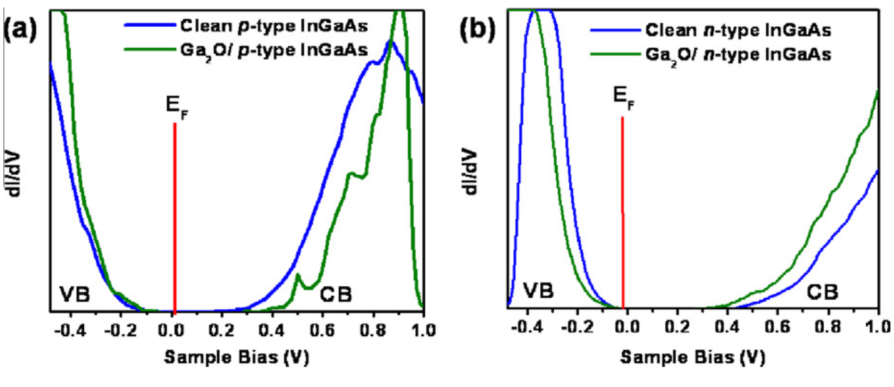

Fig. 6. Scanning tunneling spectra for the $In_{0.53}Ga_{0.47}As(0\,0\,1) - (4 \times 2)$ clean surface and Ga_2O deposited $In_{0.53}Ga_{0.47}As(0\,0\,1) - (4 \times 2)$ surface: (a) p-type sample; (b) n-type sample. For both p-type and n-type $In_{0.53}Ga_{0.47}As(0\,0\,1) - (4 \times 2)$ clean surfaces, the Fermi level (0 V) lies near the valence band maximum (VBM). After Ga_2O oxide deposition, for both p-type sample and n-type samples, the Fermi level still remain near VBM. These results indicate that the Fermi level is still pinned after Ga_2O deposition.

dimer insertion sites cannot exist on $InGaAs(0\,0\,1) - (4 \times 2)$ consistent with Ga_2O/.InGaAs(100) being both unable to form monolayer order structures and with the surface being pinned.

4. Summary

The bonding geometries of two different oxides Ga_2O and In_2O on $In_{0.53}Ga_{0.47}As(0\,0\,1) - (4 \times 2)$ were investigated using STM. The results show at low coverage, both Ga_2O and In_2O molecules bond to the As atoms at the edge of the rows. However, Ga_2O molecules also bond to preexisting Ga_2O oxide on the surface. At high full coverage with post-deposition annealing, Ga_2O oxide forms disordered structures with the large flat terraces on the surface, while In_2O oxide forms ordered structures running in the [1 1 0] direction on $In_{0.53}Ga_{0.47}As(0\,0\,1) - (4 \times 2)$. STS results show that Ga_2O oxide does not passivate the interface nor unpin the $In_{0.53}Ga_{0.47}As(0\,0\,1) - (4 \times 2)$ surface consistent with its inability to form monolayer ordered islands on the surface.

Acknowledgements

The authors would like to thank T.J. Grassman, T. Song and J.B. Clemens for very helpful discussions. J. Shen gratefully acknowledges PhD Foundation Fellowship from the Intel Corporation. This work was supported by SRC-NCRC-1437.003, the FCRP-MSD-887.011 and NSF-DMR-0706243.

References

[1] R. Chau, S. Datta, M. Doczy, B. Doyle, J. Kavalieros, M. Metz, IEEE Electron Device Letters 25 (6) (2004) 408.
[2] R. Chau, S. Datta, M. Doczy, B. Doyle, J. Jin, J. Kavalieros, A. Majumdar, M. Metz, M. Radosavljevic, IEEE Transactions on Nanotechnology 4 (2) (2005) 153.
[3] M.J. Hale, S.I. Yi, J.Z. Sexton, A.C. Kummel, M. Passlack, Journal of Chemical Physics 119 (13) (2003) 6719.
[4] W.E. Spicer, P.W. Chye, P.R. Skeath, C.Y. Su, I. Lindau, Journal of Vacuum Science & Technology 16 (5) (1979) 1422.
[5] M.L. Huang, Y.C. Chang, C.H. Chang, Y.J. Lee, P. Chang, J. Kwo, T.B. Wu, M. Hong, Applied Physics Letters 87 (25) (2005) 252104.
[6] J.J. Kolodziej, B. Such, M. Szymonski, Physical Review B 71 (16) (2005) 7.
[7] W. Melitz, J. Shen, S. Lee, J.S. Lee, A.C. Kummel, R. Droopad, E.T. Yu, Journal of Applied Physics 108 (2) (2010) 023711.
[8] J. Robertson, Applied Physics Letters 94 (15) (2009) 152104.
[9] J. Shen, E.A. Chagarov, D.L. Feldwinn, W. Melitz, N.M. Santagata, A.C. Kummel, R. Droopad, M. Passlack, Journal of Chemical Physics (2010), doi:10.1063/1.3497040.
[10] G. Binnig, H. Rohrer, Surface Science 126 (1–3) (1983) 236.
[11] G. Binnig, H. Rohrer, IBM Journal of Research and Development 30 (4) (1986) 355.
[12] G. Binnig, H. Rohrer, Reviews of Modern Physics 59 (3) (1987) 615.
[13] G. Binnig, H. Rohrer, Reviews of Modern Physics 71 (2) (1999) S324.
[14] G. Binnig, H. Rohrer, C. Gerber, E. Weibel, Physical Review Letters 50 (2) (1983) 120.
[15] C.J. Chen, Introduction to Scanning Tunneling Microscopy, Oxford University Press, 1993.
[16] J. Tersoff, D.R. Hamann, Physical Review Letters 50 (25) (1983) 1998.
[17] J. Tersoff, D.R. Hamann, Physical Review B 31 (2) (1985) 805.
[18] R.M. Feenstra, Surface Science 603 (18) (2009) 2841.
[19] R.M. Feenstra, Y. Dong, M.P. Semtsiv, W.T. Masselink, Nanotechnology 18 (4) (2007) 7.
[20] R.M. Feenstra, J.A. Stroscio, Journal of Vacuum Science & Technology B 5 (4) (1987) 923.
[21] R.M. Feenstra, J.A. Stroscio, A.P. Fein, Surface Science 181 (1–2) (1987) 295.
[22] J. Mirecki Millunchick, A. Riposan, B.J. Dall, C. Pearson, B.G. Orr, Surface Science 550 (1–3) (2004) 1.
[23] P.A. Bone, J.M. Ripalda, G.R. Bell, T.S. Jones, Surface Science 600 (5) (2006) 973.
[24] J. Shen, J.B. Clemens, E.A. Chagarov, D.L. Feldwinn, W. Melitz, T. Song, S. Bishop, A.C. Kummel, R. Droopad, Surface Science 604 (2010) 1757.
[25] P. Kruse, J.G. McLean, A.C. Kummel, Journal of Chemical Physics 113 (20) (2000) 9224.
[26] T.T. Chiang, W.E. Spicer, Journal of Vacuum Science & Technology A-Vacuum Surfaces and Films 7 (3) (1989) 724.
[27] M.J. Hale, J.Z. Sexton, D.L. Winn, A.C. Kummel, M. Erbudak, M. Passlack, Journal of Chemical Physics 120 (12) (2004) 5745.
[28] D.L. Winn, T.J. Grassman, A.C. Kummel, ECS Transactions 11 (4) (2007) 441.